Topological phases with higher winding numbers in nonreciprocal one-dimensional topolectrical circuits

S. M. Rafi-Ul-Islam,* Zhuo Bin Siu,† and Mansoor B. A. Jalil‡
Department of Electrical and Computer Engineering, National University of Singapore, Singapore

(Received 14 July 2020; accepted 8 January 2021; published 21 January 2021)

We propose the realization of higher winding number topological states in a one-dimensional system by means of a non-Hermitian, nonreciprocal topoelectrical (TE) circuit lattice. The crucial element of the circuit is a directional intercell π-phase coupling which is realized by operational amplifiers (op-amps). The phase of the coupling coefficients can be modulated by the choice of capacitive or inductive hoppings between the voltage nodes. The resulting topological state has a winding number of 2 compared to its Hermitian counterpart, which can have at most a winding number of one. Furthermore, in this system the nontrivial topological eigenmodes are localized at the edges. This localization can coexist with the non-Hermitian skin effect, the latter of which is induced by having different magnitudes of the left- and right-directional couplings. In practice, the higher winding number topological state can be distinguished from the trivial phase by the much higher resonant impedance values. Furthermore, by shunting the op-amps, we can recover the Hermiticity of the system and the conventional topological phase. The experimental accessibility and unprecedented tunability of the model parameters in our TE model provide a ready platform for the realization and detection of higher winding number topological phases in one-dimensional systems.

DOI: 10.1103/PhysRevB.103.035420

I. INTRODUCTION

Recently, higher-order topological phases [1–4] have attracted much attention due to the existence of unconventional bulk-boundary correspondence and edge states. Such higher-order topological phases are characterized by topological invariants such as the winding [5–7] and Chern numbers [8,9] and are commonly implemented in lattice models [10]. The couplings between lattice points play an important role in determining the presence of topological characteristics such as corner modes [11,12], zero modes [13,14], edge states [15,16], and hinge states [17,18].

Another class of topological systems, i.e., non-Hermitian topological systems, are also under increasing focus due to their wider array of exotic properties compared to their Hermitian counterparts [19,20]. The removal of the symmetry constraints on their couplings and the inclusion of lossy media and components [21,22] render an unprecedented degree of flexibility and tunability to these non-Hermitian systems. We consider a subset of non-Hermitian systems known as nonreciprocal non-Hermitian systems that have asymmetric couplings. The unconventional gapless edge states in nonreciprocal systems have revolutionized our understanding of condensed-matter physics, especially with regard to emerging properties such as super sensitivity [23,24], unidirectional transparency [25,26], exceptional rings [27–29], and unidirectional transport [30,31].

Nonreciprocal systems have been investigated theoretically and realized experimentally in a variety of platforms such as acoustic metamaterials [26,32], microwave resonators [33,34], photonic crystals [35–37], cold atom systems [38], and optical lattices [39]. However, all these platforms present a number of experimental difficulties and limitations, especially in fine tuning the coupling strengths, thus making them less than ideal for the study of topological phenomena. Recently, electrical circuit networks (also known as topolectrical or TE circuits [40–45]) have emerged as an alternative platform to study boundary states and other topological phenomena related to non-Hermiticity. The Hamiltonians of these circuits can be designed to mimic the lattice Hamiltonians of condensed-matter systems. In contrast to material-based platforms, TE networks offer unprecedented control and flexibility in fine-tuning and modulating the coupling coefficients. This is crucial because the nature and strength of these couplings would ultimately determine the topological properties of the whole system. Hence, such TE circuits have been widely investigated both theoretically and experimentally for various emerging fields such as Chern insulators [46], the skin effect [47,48], Weyl semimetals [40,41,45], the quantum spin-valley Hall effect [49–51], and hybrid topological insulators [52].

In this paper, we combine the two concepts of non-Hermiticity and higher-winding number phase in a one-dimensional setting. The most well-known one-dimensional system with nontrivial topology is the Su-Schrieffer-Heeger (SSH) model [53,54]. It consists of a one-dimensional array of lattice points with alternating off-diagonal coupling strengths to mimic polyacetylene. The SSH model and its many variations have been extensively studied in various platforms,

*e0021595@u.nus.edu
†elesiuz@nus.edu.sg
‡elembaj@nus.edu.sg

including ultracold atomic gases [55–57], magnetic lattices [58,59], photonic simulators [60], metamaterials [61,62], optical lattices [63,64] and TE systems [42]. However, the nontrivial topological phases in these SSH models are characterized by a winding number of one. Hence, we propose to utilize the unprecedented flexibilities afforded by TE circuit design, including the introduction of non-Hermiticity into the circuit to achieve the realization of higher-winding number phases (HWNPs) in a one-dimensional system.

We consider a TE network consisting of electrical components such as operational amplifiers (op-amps), capacitors, and inductors. The capacitors (inductors) connect electrical nodes with reciprocal positive (negative) coupling coefficients, while op-amps are used to obtain nonreciprocal directional coupling between the nodes. Here, a nonreciprocal coupling between two lattice nodes a and b is such that the coupling coefficient of the hopping from a to b differs from the complex conjugate of the reverse hopping from b to a. These nonreciprocal couplings break the Hermiticity of the circuit Hamiltonian. A higher winding number of 2 with an accompanying pair of gapless edge states appear in the circuit's admittance band dispersion when the nonreciprocal hopping between pairs of nodes has equal strength but a relative phase difference of π between the two directions. The edge states in our nonreciprocal TE system exhibit what we refer to as the higher-winding number topological surface states (HWTSSs). This differs from the conventional skin effect in two key aspects: (i) the system carries a higher winding number of 2 rather than the winding number of 1 in non-Hermitian systems with the conventional skin effect and (ii) in HWTSSs, boundary localization is exhibited by a limited number (two pairs) of topological eigenmodes and this number is independent of system size. However, an imbalance in the magnitude of the nonreciprocal couplings in the circuit model will result in the emergence of the conventional non-Hermitian skin effect (NHSE), which coexists with the HWTSS. In the conventional NHSE, the modes in the bulk bands are also localized at the boundaries and thus the number of localized modes increases with system size. In practical measurements, the HWNP can be distinguished from the trivial phase by the much higher values of the impedance readout taken between two boundary nodes. Its impedance spectrum attains its peak value at the exceptional points which mark the degeneracy points of the eigenenergies. By replacing the op-amps in the circuit with capacitors or inductors, one can restore the reciprocal TE model with its corresponding topological edge states with a winding number of one similar to that of the SSH model. In summary, we propose a general TE setup where gapless topological phases with a winding number of 2 (one) can be achieved in nonreciprocal (reciprocal) circuit frameworks simply by enabling (shunting) the op-amp components which afford directional phase-dependent couplings between the circuit nodes.

II. MODEL AND RESULTS

We begin by describing a TE circuit which can be regarded as an analog to a condensed-matter tight-binding (TB) lattice system. The analogy between the two is as follows (for details, see Ref. [41]): Each electrical node in a TE circuit is analogous to a TB lattice site and the node voltage in the former is analogous to the wave function at a lattice site in the latter. The inductive, capacitive, and nonreciprocal couplings due to inductors, capacitors, and op-amps connecting the voltage nodes in a TE circuit play the role of the intersite hopping coefficients of the TB lattice. The electrical Kirchhoff's laws governing the voltage distribution across the nodes in terms of the internode electrical connections can be written in analogous form to the quantum mechanical TB Schrödinger equation $H\psi = E\psi$. In TE circuits, the role of the eigenenergy is played by a common admittance coupling of all the nodes to the ground. The admittance of a capacitor C and an inductor L at a given ac frequency ω are $i\omega C$ and $-i/(\omega L)$, respectively. From the perspective of admittance, an inductor effectively acts as a negative capacitance. Thus, in what follows, we may refer to inductances as negative capacitances for simplicity. With the above analogies, the TE model can be mapped to any lattice Hamiltonian of a condensed-matter system.

We consider a one-dimensional TE circuit composed of capacitors and inductors, with a unit cell consisting of four electrical nodes labeled P, Q, R, and S, as indicated by the dashed boxes in Fig. 1(a). The nodes in our TE model are connected by two different types of coupling, namely, reciprocal and nonreciprocal, which are indicated by orange and purple lines, respectively, in the same figure. All electrical nodes within a unit cell are connected to their nearest neighbors by reciprocal couplings, i.e., $C_{i,j} = C_{j,i}$ with $i, j \in \{P, Q, R, S\}$ where $C_{i,j}$ is the coupling associated with the hopping from nodes i to j. The reciprocal couplings may have positive or negative signs, which are realized by capacitors or inductors, respectively. However, the intercell couplings are nonreciprocal, i.e., $C_{i,j} \neq C_{j,i}$ (with nodes i and j belonging to adjacent unit cells), thus breaking the Hermiticity of the Hamiltonian. In our particular TE circuit, the nonreciprocal couplings in the two hopping directions have the same magnitude but a phase difference of π between them (they are in antiphase), i.e., $C_{i,j} = -C_{j,i}$. This can be readily implemented by using op-amp-based negative impedance converter (NIC) with current inversion [see Fig. 1(c)]. Because the input terminals of an ideal op-amp are connected via a very high impedance, virtually no current will flow between its two input terminals, v_+ and v_- [see Fig. 1(c)]. This basic nonreciprocal circuit unit reverses the current flow direction once the acting node (i.e., where the ac current or voltage source is connected) switches, hence introducing a directional phase shift of π between voltage and current. Thus, this NIC would realize a directional anti-phase (π phase difference) coupling between the two nodes. This nonreciprocal coupling results in non-Hermitian terms in the TE model that would lead to interesting consequences such as the HWNP (as we shall see later). Finally, the grounding mechanism for each electrical node is shown in Fig. 1(b), where all nodes are connected to ground by a common inductance L and a common capacitance C. In parallel to C and L, the Q and S nodes are also connected to ground by another capacitance C_1, while nodes P and R have the same coupling strength to ground but with opposite signs, i.e., $-C_1$ (achieved with the appropriate inductive coupling). The voltages at the nodes in an electrical network are related by Kirchoff's current law, which states that the net current

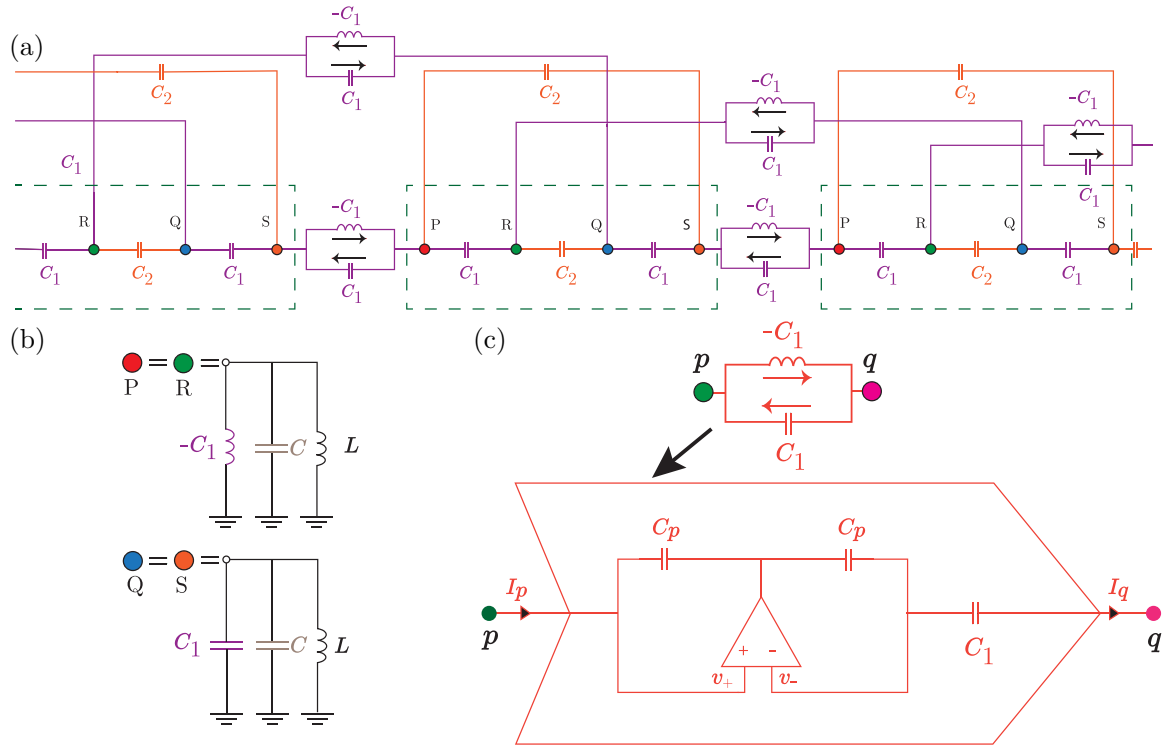

FIG. 1. (a) Schematic one-dimensional nonreciprocal TE circuit consisting of op-amps, inductors, and capacitors, which is designed to host a higher-order topological phase. The dashed boxes indicate the elementary unit cells with reciprocal hopping within nodes of same cell and nonreciprocal π-phase coupling between nodes of neighboring cells. (b) Grounding mechanism of electrical nodes. The common inductor L determines the diagonal elements of the Hamiltonian matrix and thus modulates the resonant frequency. The common capacitance C plays the role of the TB eigenenergy in the TE equivalent of the Hamiltonian. (c) The elementary unit consisting of op-amp that gives rise to the π-phase difference directional coupling via negative impedance converter with current inversion. The op-amp has a unity gain factor with virtually shorted positive (v_+) and negative (v_-) input terminals. No current flows between v_+ and v_-, so $C_{p,q} = -C_{q,p}$.

flowing in or out of a node is zero. At the ith node, we have

$$0 = \sum_j C_{ij}\frac{d}{dt}(V_i - V_j) + \frac{1}{L}\int V_i dt + (C + \tilde{C}_i)\frac{d}{dt}V_i, \quad (1)$$

where $\tilde{C}_i$ is $-C_1$ at a P/Q node and C_1 at an R/S node, V_i is the potential at the ith node, and L and C are the common grounding inductance and capacitance. Assuming an ac current flow with an $\exp(i\omega t)$ time dependence, Eq. (1) can be cast into the form of

$$CV_i = \sum_j C_{ij}(V_j - V_i) + \frac{1}{\omega^2}L - \tilde{C}_i V_i. \quad (2)$$

Applying Eq. (2) at all the voltage nodes, the resulting set of equations can be written in the form of

$$C\mathbf{v} = \mathbf{H}\mathbf{v}, \quad (3)$$

where $\mathbf{v}$ is the vector of the node voltages and $\mathbf{H}$ is the matrix constructed from the right-hand side of Eq. (2). Equation (3) is the TE equivalent of the Schrödinger equation $H\psi = E\psi$, where C and $\mathbf{v}$ play the roles of the energy eigenvalue E and eigenfunction ψ, respectively. We shall refer to matrix $\mathbf{H}$ in Eq. (3) as the Hamiltonian of the TE circuit (we will drop the boldface notation for simplicity) and, by reference to the Schrödinger equation, we would write the eigenvalue C as E. In a periodic TE circuit, the values of E which satisfy Eq. (3) form a continuum and the Bloch theorem can be invoked to express the position dependence of the voltage profile, which takes the form of $\exp(ik_x n)$, where k_x and n are dimensionless quantities representing the wave vector and unit cell index, respectively. The E-k_x dispersion relation then relates the value of the common grounding capacitance C $(= E)$ to the spatial wavelengths (related to k_x) of the allowed TE voltage profiles, i.e., those that are consistent with Kirchhoff's current law.

Explicitly, the four-band Hamiltonian for the TE circuit in Fig. 1(a) can be written as

$$H(k_x) = \begin{pmatrix} \left(\frac{1}{\omega^2 L} - C_1 - C_2\right)\sigma_0 & h(k_x) \\ h(-k_x) & \left(\frac{1}{\omega^2 L} - C_1 - C_2\right)\sigma_0 \end{pmatrix}, \quad (4)$$

where $h(k_x) = C_1\sigma_0 + C_2\sigma_x - iC_1 e^{-ik_x}\sigma_y$ and σ_i is the ith Pauli matrix. The common inductor L therefore acts as a global offset to the eigenvalues of $H(k_x)$. L is introduced so the diagonal elements of Eq. (4) can be set to zero for convenience by setting the frequency of the TE circuit to the resonant frequency of $\omega_r = 1/\sqrt{L(C_1 + C_2)}$. At the resonant frequency, the Hamiltonian possesses chiral symmetry as expressed by the relation $\mathcal{C}_h H(k_x)\mathcal{C}_h^{-1} = -H(k_x)$, where the chiral reversal operator $\mathcal{C}_h = \mathbf{I} \otimes \sigma_z$. The chiral symmetry guarantees a symmetric admittance spectrum about $E = 0$ where every state at a given k_x with eigenvalue E has a counterpart at the same k_x with eigenvalue $-E$. The chiral symmetry is broken at off-resonant frequency, i.e., $\omega \neq \omega_r$. The Hamiltonian is also $\mathcal{PT}$ symmetric, i.e.,

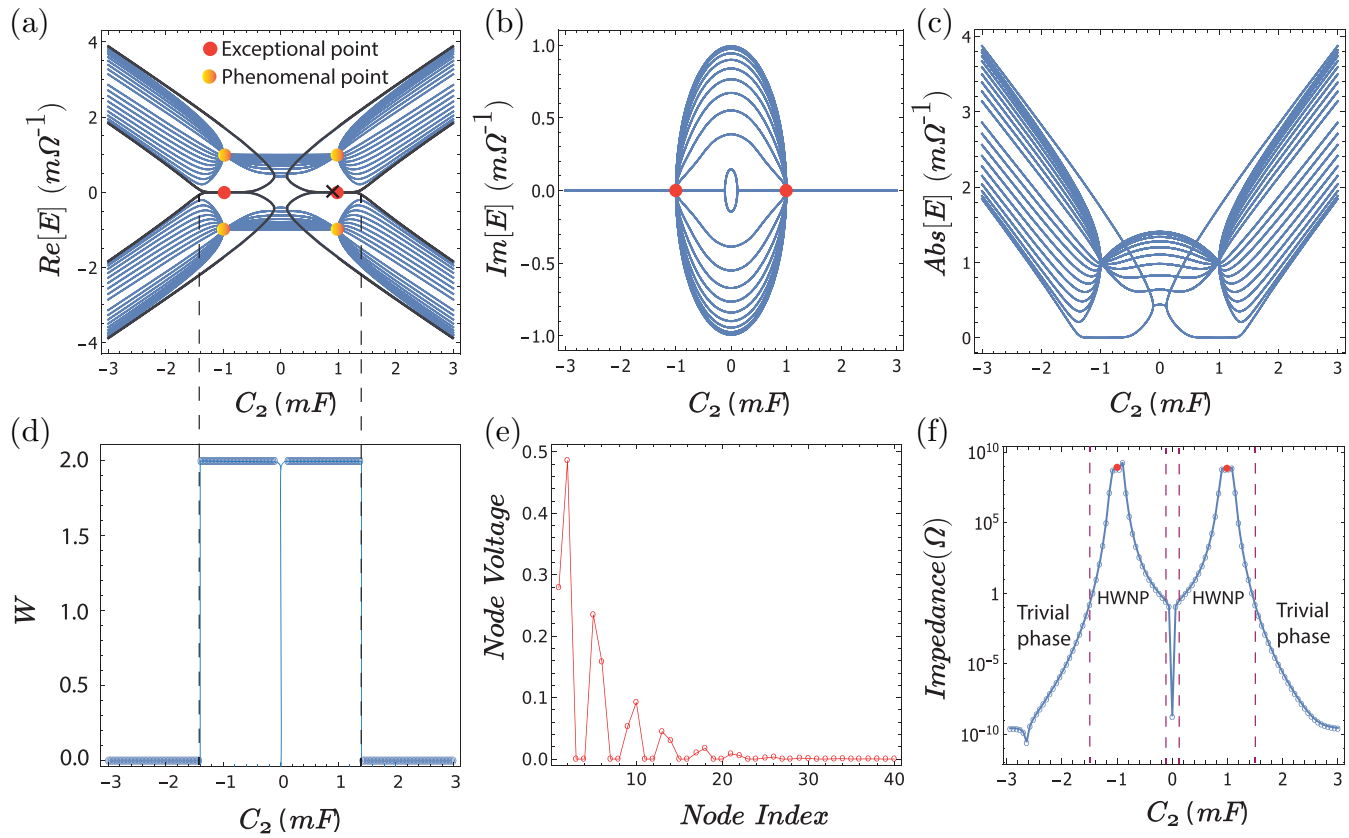

FIG. 2. (a)–(c) Admittance spectrum of the nonreciprocal TE circuit under consideration. We consider a finite circuit with $p = 20$ unit cells and apply open boundary conditions. The spectrum is plotted as a function of coupling capacitance C_2 with $C_1 = 1$ mF for (a) real parts, (b) imaginary parts, and (c) absolute values of the admittance spectrum. The bold lines in (a) indicate the edge states. (d) Topological index or winding number W as a function of C_2. W takes the discrete values of two for $|C_2/C_1| < \sqrt{2}$ and zero for $|C_2/C_1| > \sqrt{2}$. (e) Voltage profile of one of the nearly zero-admittance eigenstates at $C_2 = 0.9$ mF, indicated with a cross in panel (a), as a function of the transverse position. All the nearly-zero admittance states are localized in the vicinity of one of the boundaries, indicating that these are edge states. (f) The spectrum of the impedance taken between the terminal nodes of the TE circuit. The impedance peaks (marked by red dots) occur at the exceptional points located at $C_2 = \pm C_1$. The HWNP is characterized by high impedance readout. The impedance falls drastically by orders of magnitude beyond $|C_2/C_1| > \sqrt{2}$ corresponding to the trivial phase.

$\mathcal{PT}H(k_x)\mathcal{P}^{-1}\mathcal{T}^{-1} = H(k_x)$, where the parity inversion operator $\mathcal{P} = \mathbf{I} \otimes \sigma_x$ and the time-reversal operator $\mathcal{T}$ is complex conjugation. Moreover, the Hamiltonian in Eq. (4) preserves mirror rotational symmetry at resonant frequency with $\mathcal{M}_\mathcal{R} = \sigma_x \otimes \sigma_0$ that satisfies $\mathcal{M}_\mathcal{R}H(k_x) = H(-k_x)\mathcal{M}_\mathcal{R}$. Interestingly, $\mathcal{M}_\mathcal{R}$ commutes with both the chiral and time-reversal symmetry operators. The eigenvalues of the Hamiltonian in Eq. (4) at the resonant frequency are given by

$$E_\pm = \pm\sqrt{C_2^2 \pm 2\sqrt{C_1^2\left(C_2^2 - C_1^2\right)\cos^2 k_x}}. \tag{5}$$

The admittance spectra (note that admittance is the TE analog of eigenenergy) of the nonreciprocal Hamiltonian is, in general, complex but becomes real at $|C_2| > |C_1|$. Figure 2 shows the complex admittance spectra corresponding to the finite TE system under consideration with open boundary conditions (OBCs). The directional π-phase couplings support edge states when $|C_2| < \sqrt{2}|C_1|$ [the range being demarcated by vertical dashed lines in Fig. 2(a)]. In a typical (first-order) topological insulator (e.g., the surface state of Bi_2Se_3), there are, at a given wave vector $\vec{k}$, only two topological surface states, one of which is holelike and the other particlelike. Interestingly, our TE system can harbor more than two topological edge states at each value of k_x, where such states exist. (The eigenvalues of H are actually twofold degenerate, so each visible line in the figure represents two states. The twofold degeneracy is due to the $\mathcal{PT}$ symmetry of the Hamiltonian.) This is a manifestation of the HWNP, which will be further confirmed by explicit calculation of its winding number. Another interesting feature occurs at $|C_1| = |C_2|$, where the imaginary part of the admittance spectra vanishes [see Fig. 2(b)] while the real part of the spectra coalesces into three distinct points [see Fig. 2(a)]. One of these points occurs at zero admittance and is known as an exceptional point while the other two occur at nonzero admittance $E = \pm C_1$ and are called phenomenal points [65]. When $|C_2| > |C_1|$, the admittance dispersion becomes purely real [see Fig. 2(b)], indicating that the eigenvectors respect $\mathcal{PT}$ symmetry. In the vicinity of $|C_2| \geqslant \sqrt{2}|C_1|$, the real part of lowest absolute admittance bands split prominently into two distinct bands which then diverge with the further increase of $|C_2|$. Interestingly, in the vicinity of $C_2 \approx 0$, the Hamiltonian becomes topologically trivial and does not host any edge modes. One

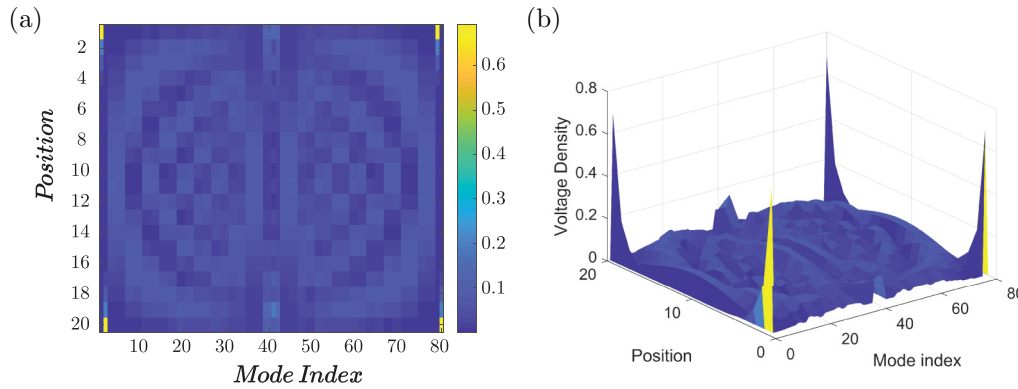

FIG. 3. Two representations of the node voltage density distribution of the nonreciprocal TE circuit given by Eq. (4) with open boundary condition in the x direction. (a) depicts the density plot in the 2D plane as a function of the mode index and the position of the voltage nodes. (b) shows the surface plot of the same information as in (a) to emphasize that only the non-Hermitian nontrivial states are localized at the edges. The parameters used are $C_1 = 1$ mF and $C_2 = 0.5$ mF.

may be curious to know about the localization of the eigenstates of our π-phase nonreciprocal TE system. We find that for $C_2 < \sqrt{2}C_1$, the eigenmodes with the largest magnitudes of real admittance and the nearly zero-admittance modes are highly localized at the edges [see Fig. 2(e)]. (The apparently flat dispersion relation in Figs. 2(a) and 2(b) for the range $|C_2/C_1| < \sqrt{2}$ is not exactly a flat line but has a small finite separation between the hole and particle states not visible in the scale of the figure, except at the two exceptional points where the bands touch.) At $C_2 > \sqrt{2}C_1$, no nearly zero-admittance edge states exist.

A. Topological invariant

We next consider the topological invariant associated with our system in order to characterize and confirm its topological phases. The topological characteristics of a nonreciprocal system can be characterized by the winding number [66]. The non-Hermitian winding number associated with the Hamiltonian of Eq. (4) is given by

$$\chi_{\pm} = \frac{i}{2\pi}\int_{\mathrm{GBZ}} \frac{\langle\lambda_{\pm}|\partial_k\phi_{\pm}\rangle}{\langle\lambda_{\pm}|\phi_{\pm}\rangle}dk_x. \tag{6}$$

Note that the integration is, in general, performed over a complex k_x contour when the NHSE occurs in the system. GBZ denotes the generalized complex Brillouin zone and $\chi_{\pm}$ denotes the winding number for $h(+k_x)$ and $h(-k_x)$ in Eq. (4), respectively. $\langle\lambda_{\pm}|$ and $|\phi_{\pm}\rangle$ are the left and right admittance eigenstates of $h(\pm k_x)$, respectively. This yields the total winding number of the TE circuit as

$$W = \frac{\chi_+ - \chi_-}{2}. \tag{7}$$

One can regard the topological index W in one dimension as characterizing the number of multiples of 2π the phase of the eigenstate changes as k_x is varied from one edge of the one-dimensional Brillouin zone to the other [5]. The variation of W with C_2 is shown in Fig. 2(d). The plot shows that in the presence of the π-phase nonreciprocal coupling, our TE circuit exhibits a winding number $W = 2$ when $0 < |C_2| < \sqrt{2}|C_1|$, and zero winding number ($W = 0$), indicating a trivial phase for $|C_2| > \sqrt{2}|C_1|$ and $C_2 = 0$. The variation of W with C_2 is consistent with the presence ($W = 2$) and absence ($W = 0$) of nearly zero-admittance edge states evident in the admittance spectra presented in the previous section.

B. Higher-winding number topological surface states

Our system with equal magnitude of nonreciprocal coupling strength but having a π phase difference [i.e., Eq. (4)] does not exhibit the conventional NHSE (i.e., complete localization of both the bulk and edge modes; we will show the emergence of NHSE in the presence of unequal nonreciprocal couplings in the next section).

We prove the presence of the HWTSSs in our system by evaluating the TE analogs of the particle densities directly. Figure 3 shows the spatial distributions of the voltage (i.e., the TE equivalent of the particle density) for all of the eigenmodes for a finite system with 20 repeating units and setting the coupling capacitance to an exemplary value of $C_2 = 0.5$ mF. Figure 3 shows that except for the four topologically nontrivial states (modes 1, 2, 79 and 80 above), none of the other states are localized at the edges (see Supplemental Material Note 4 [67] for more details).

In the conventional skin effect exhibited by the non-Hermitian SSH model, all the eigenstates exhibit boundary localization. Furthermore, both the non-Hermitian SSH model and its Hermitian counterparts carry the same winding number of unity. By contrast, in our higher-order non-Hermitian system, boundary localization is exhibited by only two pairs of eigenstates, while the rest remain delocalized and form bulk bands. Furthermore, the non-Hermitian system exhibits a higher topological index of two [68] compared to the corresponding topological index of unity of its Hermitian counterpart [69]. Furthermore, the admittance variations in the complex plane for the OBC and periodic boundary condition (PBC) look similar yet are not completely identical (see Supplemental Material Note 2 and Supplemental Material Fig. 3). More explicitly, for the topologically nontrivial states the admittance spectra shows pronounced differences while for the trivial states, the admittance distribution look similar and almost identical. The nontrivial states constitute the aforementioned HWTSSs and occur in a non-Hermitian system

with a higher topological index and in which only some of the eigenstates exhibit boundary localization. The origin of this HWTSS stems from the additional circuit symmetries (i.e., rotational and $\mathcal{PT}$ symmetries in our model) as well as the system's non-Hermiticity induced by the nonreciprocal couplings. On the other hand, the conventional skin effect, described hitherto, owes its origin to the intrinsic non-Hermitian topology of the corresponding systems [70,71].

C. Impedance spectrum—a signature of higher-winding number topological phase

Experimentally, the topological character of our TE circuit can be characterized by the impedance between its terminal nodes. The impedance between two arbitrary nodes denoted as α and β can be obtained by measuring the voltage difference between these when a unit current is flowing from one node to the other. Consider our nonreciprocal TE circuit with a finite number p of unit cells (i.e., total number of nodes is $N = 4p$). The circuit Hamiltonian would have N eigenvalues and we denote the jth eigenvalue as κ_j and its corresponding left and right eigenvectors as $\langle\lambda_j|^\dagger \simeq (\lambda_{j1}, \lambda_{j2}, ..., \lambda_{jN})$ and $|\phi_j\rangle \simeq (\phi_{j1}, \phi_{j2}, ..., \phi_{jN})^{\mathrm{T}}$, respectively. $|\lambda_i\rangle$ and $|\chi_j\rangle$ are not mutually orthogonal when $i \neq j$. Therefore, the impedance the α and β nodes is given by [72]

$$Z_{\alpha\beta} = \sum_{j=1}^{N} \frac{\lambda_{j\alpha}^{*}\phi_{j\alpha} - \phi_{j\alpha}\lambda_{j\beta}^{*} + \lambda_{j\beta}^{*}\phi_{j\beta} - \phi_{j\beta}\lambda_{j\alpha}^{*}}{\kappa_j\langle\lambda_j|\phi_j\rangle}. \quad (8)$$

An important characteristic of Eq. (8) is that the impedance would be extremely large if any of the admittance eigenvalues are infinitesimally small. The impedance can thus serve as an experimental signature for the topologically nontrivial zero-admittance edge states. We show the impedance distribution for the our nonreciprocal one-dimensional TE circuit in Fig. 2(f), in which high impedances states coincide with the nontrivial topological phase (for $0 < |C_2| < \sqrt{2}|C_1|$) and much lower impedance states for the trivial phase (for $|C_2| > \sqrt{2}|C_1|$) [cf. Fig. 2(d)]. Note that the winding number reaches zero at $C_2 = 0$ [see Fig. 2(d)], indicating a phase transition at this particular point, and this is correspondingly marked by a sharp decrease in the impedance at that point [see Fig. 2(f)]. In addition, we can also identify the exceptional points by peaks in the impedance spectrum in Fig. 2(f).

D. Conventional non-Hermitian skin effect

In the following section, we will show that our model can be made to exhibit the NHSE by modifying the circuit model such that the left- and right-going coupling strengths are of opposite signs and have different magnitudes. We will also show in detail the different signatures of NHSE in the modified circuit (voltage distribution for the nontrivial and trivial bulk modes, loci of eigenvalues in complex plane for OBCs and PBCs, as well as analytical derivation of the prerequisites for the onset of NHSE). This circuit modification neither affects the higher winding number of 2 nor the appearance of two pairs of topological edge states in the circuit that were present in the original circuit.

Explicitly, to realize the NHSE in our circuit model, we modify the circuit connections shown in Fig. 1 in such a way that the left and right directional couplings in the nonreciprocal segments are not equal (i.e., $|C_{\mathrm{left}}| \neq |C_{\mathrm{right}}|$). The modified circuit with nonequal directional couplings is shown in Fig. 1 of the Supplemental section.

The Laplacian of the modified circuit can be obtained by replacing the usual Bloch factor of e^{ik_x} in the original circuit (where $|C_{\mathrm{left}}| = -|C_{\mathrm{right}}| = C_1$) with $\beta = \alpha e^{ik_x}$, where the non-Bloch attenuation factor $\alpha = \sqrt{\frac{|C_{\mathrm{left}}|}{|C_{\mathrm{right}}|}}$. The modified circuit Laplacian at the resonant frequency condition can be rewritten as

$$H_{\mathrm{mod}}(k_x) = i\omega\begin{pmatrix} 0 & h_m(k_x) \\ h_p(k_x) & 0 \end{pmatrix}, \quad (9)$$

where $h_m(k_x) = C_1\sigma_0 + C_2\sigma_x + iC_{\mathrm{left}}\alpha^{-1}e^{-ik_x}\sigma_y$ and $h_m(k_x) = C_1\sigma_0 + C_2\sigma_x + iC_{\mathrm{right}}\alpha e^{ik_x}\sigma_y$. The admittance eigenvalues of the Laplacian of Eq. (9) at resonant frequency are given by

$$E_{\pm} = \pm\sqrt{\left(C_1^2 + C_2^2 - C_{\mathrm{left}}C_{\mathrm{right}}\right) \pm 2\sqrt{C_2^2(C_{\mathrm{left}}e^{-ik} - C_{\mathrm{right}}e^{ik})^2 - C_1^2(C_{\mathrm{left}}e^{-ik} + C_{\mathrm{right}}e^{ik})^2 + 4C_1^2C_2^2}}. \quad (10)$$

We plot the complex admittance dispersion for the modified circuit model described by Eq. (9) for a finite system with OBCs. Figures 4(a) and 4(b) show the real and imaginary admittance eigenvalues, respectively. We find well-defined nontrivial edge states for $C_{\lambda-} < C_2 < C_{\gamma-}$ and $C_{\gamma+} < C_2 < C_{\lambda-}$, where $C_{\gamma\pm} = \pm\sqrt{C_1^2 - C_{\mathrm{left}}C_{\mathrm{right}}}$ and $C_{\lambda\pm} = \pm\sqrt{C_1^2 + C_{\mathrm{left}}C_{\mathrm{right}}}$. We also calculate the generalized (non-Bloch) winding number (W) as a function of coupling capacitance C_2, as shown in Fig. 4(c). The winding number of the modified circuit takes the discrete values of two and zero for the nontrivial and trivial regions, respectively. The modified circuit thus exhibits a higher winding number just like the original circuit.

The introduction of a factor of $\alpha \neq 1$ in Eq. (9) can be interpreted as the replacement of the allowed values of k_x whose linear superpositions would satisfy the OBCs in a finite-sized system in the original TE system by $k_x - i\ln\alpha$ in the modified TE circuit. As a result, for $|C_{\mathrm{left}}| < |C_{\mathrm{right}}|$, the non-Bloch multiplication factor (α) takes a value less than one, which implies that the square of the node voltages are localized at the vicinity of the leftmost node of our modified nonreciprocal circuit (see Supplemental Material Note 3 for details). We find that the topologically trivial modes decay exponentially away from the leftmost node, as shown in Fig. 4(d), which shows the spatial distribution of the node voltages for the eigenmodes of a finite system with 20 repeating units and having the same parameters as that in Fig. 4(a), and $C_2 = 1.1$ mF. As

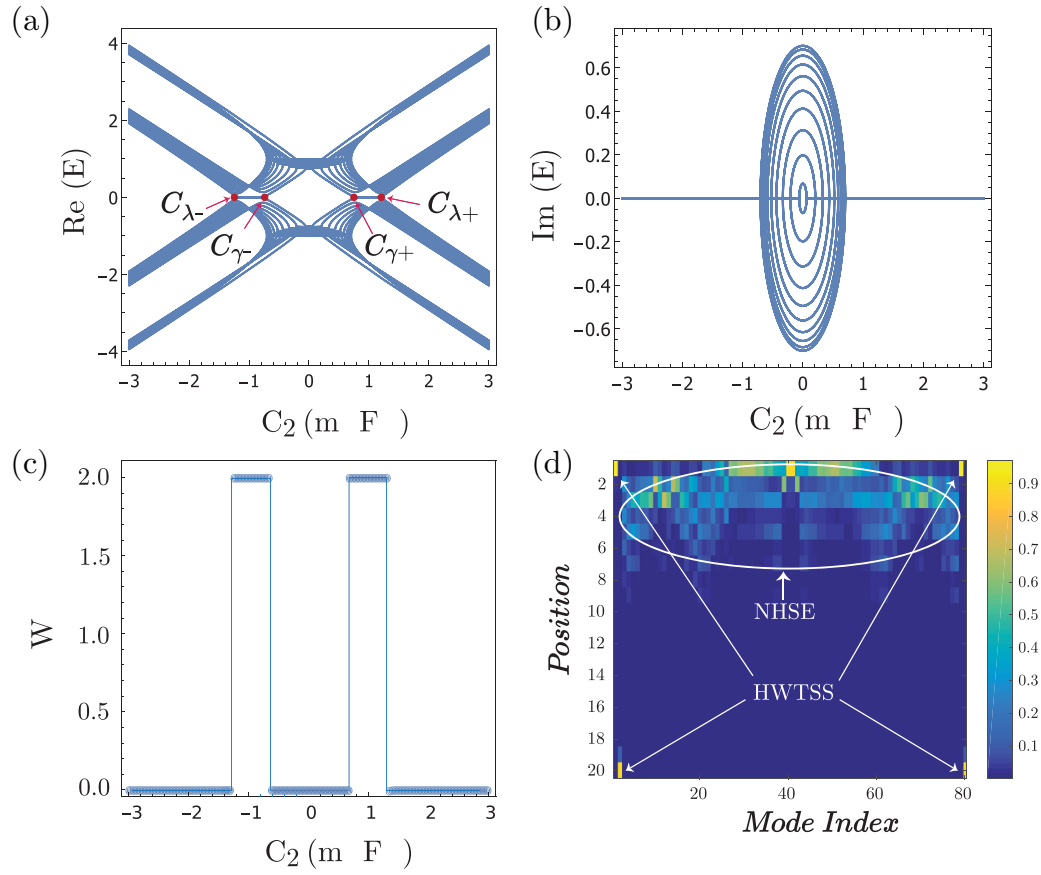

FIG. 4. (a), (b) Admittance dispersion of the modified nonreciprocal TE circuit described in Eq. (9), where the directional couplings are not equal (i.e., $|C_{\text{left}}| \neq |C_{\text{right}}|$). We consider a finite circuit with 20 unit cells and apply open boundary conditions. The spectrum is plotted as a function of coupling capacitance C_2 with $C_1 = 1$ mF, $C_{\text{left}} = 0.5$ mF and $C_{\text{right}} = 1$ mF for (a) real parts and (b) imaginary parts. (c) Topological index or non-Hermitian winding number W as a function of C_2. W takes the discrete values of two for nontrivial and zero for trivial regions. (d) Node voltages as a function of the eigenmode index and the position of the index nodes for a 20 repeating unit-wide system with OBC and $C_1 = 1$ mF, $C_2 = 1.1$ mF, $C_{\text{left}} = 0.5$ mF and $C_{\text{right}} = 1$ mF, exhibiting the coexistence of the NHSE and the HWTSS.

expected from the winding number of 2, there are two pairs of topologically nontrivial modes, namely, modes 1, 2, 79, and 80, which can be distinguished from the other states by their being localized to a larger extent. In particular, modes 2 and 80 are localized at the opposite edges from the remaining states. This is not unexpected because the topologically nontrivial states are robust to small perturbations, such as the breaking of the equality between the magnitudes of the left and right directional states, which give rise to the NHSE. The HWTSS hence coexists with the NHSE.

For another confirmation of the presence of NHSE in the modified circuit model, we plot and compare the loci spanned by the admittance eigenvalues in the complex plane for both the OBC and the PBC [see Supplemental Figs. 2(a)–2(c) corresponding to three different sets of circuit parameter values]. Interestingly, the admittance loci are completely different when the boundary conditions are changed from OBC to PBC. The nonidentical eigenvalue distributions under the different boundary conditions indicate the presence of the NHSE (see Supplemental Material Note 2 for details).

E. Reciprocal TE model and recovery of first-order topological phase

In this section, we show that the replacement of the directional π-phase couplings by reciprocal ones would recover the conventional topological insulating phase with a winding number of 1 in the TE circuit. Without the directional π-phase coupling, the circuit Hamiltonian in Eq. (4) is modified to

$$L_2(k_x) = i\omega \begin{pmatrix} \left(\frac{1}{\omega^2 L} - C_1 - C_2\right)\sigma_0 & h_2(k_x) \\ h_2(-k_x) & \left(\frac{1}{\omega^2 L} - C_1 - C_2\right)\sigma_0 \end{pmatrix}, \tag{11}$$

where $h_2(k_x) = C_1\sigma_0 + (C_2 + C_1 e^{-ik_x})\sigma_x$. Equation (11) corresponds to the replacement of the two op-amps in Fig. 1 by a single capacitor C_1. Thus, the intercell coupling becomes reciprocal and the Hamiltonian recovers its Hermiticity.

For the nonreciprocal TE system, we found that the admittance spectrum could serve as an experimental marker for the topological state of a TE system. The same can be said for the admittance dispersion for the reciprocal TE system, which is plotted as a function of C_2 in Fig. 5(a). The Hermiticity of the Hamiltonian results in a real dispersion relation [see Fig. 5(a)].

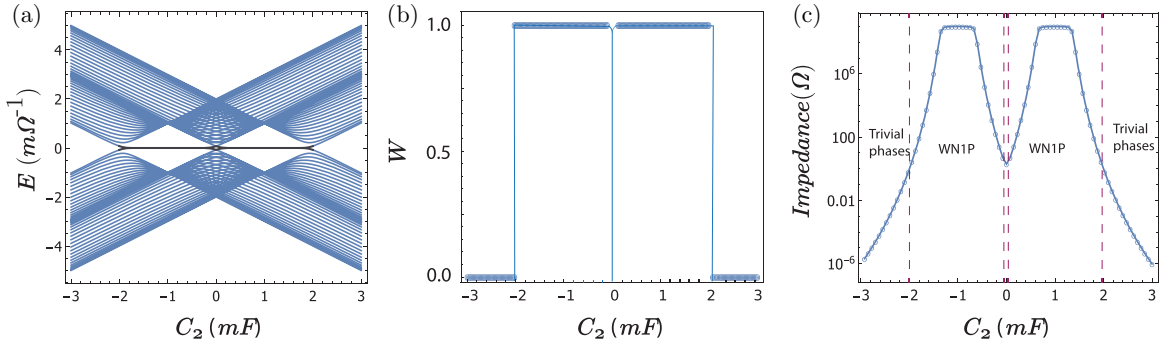

FIG. 5. (a) Admittance spectrum of a reciprocal one-dimensional TE circuit. We consider a finite TE circuit of $p = 20$ unit cells under open boundary conditions. The spectrum is plotted as a function of C_2, with $C_1 = 1$ mF. The bold lines in (a) represent the edge states. In the absence of directional π-phase coupling, the Hamiltonian of the TE circuit reverts to having a real energy spectrum with the trivial phase and a phase with a winding number of 1 (WN1P). (b) Winding number for the reciprocal TE circuit showing the WN1P for $0 < |C_2| < 2C_1$ with $W = 1$ and a trivial phase with $W = 0$ elsewhere. (c) Impedance spectrum as a function of C_2. In contrast to the nonreciprocal TE circuit, there are broader peaks centered at $C_2 = \pm C_1$, with no exceptional points in the vicinity. The WN1P and trivial phases are distinguished by high and low impedance readouts, respectively.

There exist nearly zero-admittance edge states for $|C_2/C_1| < 2$, marked by the dark horizontal lines at $E = 0$ in the dispersion plot. These edge states correspond to a topological phase with a winding number of unity [WN1P, see Fig. 5(b)]. There are only two topological edge states, one holelike and the other particlelike, at each value of k_x where these edge states exist. By contrast, in the second-order non-Hermitian system in Figs. 2(a) and 2(c), four such edge states occur at each value of k_x. At $|C_2/C_1| > 2$, the system switches to the topologically trivial phase with a winding number of 0 [see Fig. 5(b)]. Thus, there are topological phase transitions at $|C_2/C_1| = 2$ between the trivial and topological insulating phases. This recalls the standard SSH model [42,56] where topological phase transition occurs when the intracell and intercell couplings are equal (i.e., $|C_2/C_1| = 1$). In Fig. 5(c), we plot the impedance between two terminal nodes of the reciprocal TE circuit at the resonant frequency as a function of C_2. There are several main differences compared to the corresponding spectrum of the HWNP shown in Fig. 2(f). First, the impedance spectrum of the first-order topological phase of the reciprocal TE circuit exhibits two broad peaks centered at $C_2 = \pm C_1$, which extends up to $|C_2/C_1| = 2$ that marks the boundaries with the trivial phase. Thereafter, the impedance readout falls sharply when the system enters the trivial phase [see Fig. 5(c)]. In contrast, the impedance spectrum of the second-order topological phase of the nonreciprocal TE system shows two much sharper peaks at $|C_2/C_1| = \sqrt{2}$. In addition, although the peak impedance values for both TE systems are of comparable magnitude, the ratio of impedance values for the topological and trivial phases is much larger for the nonreciprocal HWNP TE system compared to the reciprocal system [cf. Figs. 2(f) and 5(c)].

III. CONCLUSIONS

In summary, we have demonstrated the emergence of a HWNP in a one-dimensional nonreciprocal TE circuit. The nonreciprocity arises from directional π-phase coupling realized by means of op-amps. The HWNP is confirmed analytically by its winding number of 2 and is also characterized by several distinct characteristics: (i) features of its admittance spectrum, such as exceptional and phenomenal points and edge states; (ii) heightened impedance readout between terminal points for the higher-order zero-admittance edge states, which are orders of magnitude higher than that of the trivial phase; and (iii) it exhibits what we term as HWTSSs, in which there is more than one pair of topological edge states localized at the boundaries. The HWTSS can coexist with the NHSE, which can be restored simply by taking nonequal directional couplings. The HWTSSs in this case exhibit a higher degree of localization than the trivial states and two of them are localized at the opposite edge from all the other states. Interestingly, the TE system can be readily switched from a HWNP to the conventional WN1P, the latter akin to the topological state in the standard SSH model. This is accomplished by replacing the directional coupling through the op-amps with the reciprocal coupling of a conventional capacitor, which restores the Hermiticity of the Hamiltonian and ensures a real admittance spectrum. The resulting WN1P phase has a winding number of unity and exhibits lower impedance ratios compared to its HWNP in the nonreciprocal TE circuit. Our work demonstrates the flexibility and utility of the TE circuit platform in realizing transitions between various topological phases from the trivial order to the HWNP, all achievable by controlling the type and strength of couplings afforded by standard circuit elements. In addition, it was recently noted that a non-Hermitian multiband Hamiltonian may be interpreted as a collection of distinct subgeneralized Brillouin zones for each band [73]. Our system may, after suitable modifications, serve as a platform for exploring the physics induced by these multiple subgeneralized Brillouin zones.

ACKNOWLEDGMENTS

This work is supported by the Ministry of Education (MOE) Tier-II Grant No. MOE2018-T2-2-117 (NUS Grants No. R-263-000-E45-112 and No. R-398-000-092-112), MOE Tier-I FRC grant (NUS Grant No. R-263-000-D66-114), and other MOE grants (NUS Grant No. C-261-000-207-532 and No. C-261-000-777-532).

[1] E. Edvardsson, F. K. Kunst, and E. J. Bergholtz, Phys. Rev. B **99**, 081302(R) (2019).

[2] T. Liu, Y.-R. Zhang, Q. Ai, Z. Gong, K. Kawabata, M. Ueda, and F. Nori, Phys. Rev. Lett. **122**, 076801 (2019).

[3] M. Ezawa, Phys. Rev. B **98**, 201402(R) (2018).

[4] X.-W. Luo and C. Zhang, Phys. Rev. Lett. **123**, 073601 (2019).

[5] C. Yin, H. Jiang, L. Li, R. Lü, and S. Chen, Phys. Rev. A **97**, 052115 (2018).

[6] T. E. Lee, Phys. Rev. Lett. **116**, 133903 (2016).

[7] D. Leykam, K. Y. Bliokh, C. Huang, Y. D. Chong, and F. Nori, Phys. Rev. Lett. **118**, 040401 (2017).

[8] S. Yao, F. Song, and Z. Wang, Phys. Rev. Lett. **121**, 136802 (2018).

[9] K. Esaki, M. Sato, K. Hasebe, and M. Kohmoto, Phys. Rev. B **84**, 205128 (2011).

[10] F. K. Kunst, G. van Miert, and E. J. Bergholtz, Phys. Rev. B **97**, 241405(R) (2018).

[11] M. Ezawa, Phys. Rev. B **99**, 201411(R) (2019).

[12] S. Imhof, C. Berger, F. Bayer, J. Brehm, L. W. Molenkamp, T. Kiessling, F. Schindler, C. H. Lee, M. Greiter, T. Neupert *et al.*, Nat. Phys. **14**, 925 (2018).

[13] L. Jin and Z. Song, Phys. Rev. B **99**, 081103(R) (2019).

[14] J. M. Zeuner, M. C. Rechtsman, Y. Plotnik, Y. Lumer, S. Nolte, M. S. Rudner, M. Segev, and A. Szameit, Phys. Rev. Lett. **115**, 040402 (2015).

[15] L. Jin, Phys. Rev. A **96**, 032103 (2017).

[16] C. Yuce, Phys. Rev. A **98**, 012111 (2018).

[17] Z. Zhang, M. Rosendo López, Y. Cheng, X. Liu, and J. Christensen, Phys. Rev. Lett. **122**, 195501 (2019).

[18] W. A. Benalcazar, B. A. Bernevig, and T. L. Hughes, Phys. Rev. B **96**, 245115 (2017).

[19] C.-H. Liu, H. Jiang, and S. Chen, Phys. Rev. B **99**, 125103 (2019).

[20] X. Ni, D. Smirnova, A. Poddubny, D. Leykam, Y. Chong, and A. B. Khanikaev, Phys. Rev. B **98**, 165129 (2018).

[21] R. El-Ganainy, K. G. Makris, M. Khajavikhan, Z. H. Musslimani, S. Rotter, and D. N. Christodoulides, Nat. Phys. **14**, 11 (2018).

[22] C. Yuce, Phys. Rev. A **93**, 062130 (2016).

[23] F. K. Kunst and V. Dwivedi, Phys. Rev. B **99**, 245116 (2019).

[24] C. Sun, J. Deng, S. M. Rafi-Ul-Islam, G. Liang, H. Yang, and M. B. A. Jalil, Phys. Rev. Appl. **12**, 034022 (2019).

[25] S. Longhi, D. Gatti, and G. Della Valle, Phys. Rev. B **92**, 094204 (2015).

[26] L. Feng, Y.-L. Xu, W. S. Fegadolli, M.-H. Lu, J. E. Oliveira, V. R. Almeida, Y.-F. Chen, and A. Scherer, Nat. Mater. **12**, 108 (2013).

[27] E. M. Graefe, U. Günther, H. Korsch, and A. Niederle, J. Phys. A: Math. Theor. **41**, 255206 (2008).

[28] J. Carlström and E. J. Bergholtz, Phys. Rev. A **98**, 042114 (2018).

[29] Y. Xu, S.-T. Wang, and L.-M. Duan, Phys. Rev. Lett. **118**, 045701 (2017).

[30] C. Qin, B. Wang, Z. J. Wong, S. Longhi, and P. Lu, Phys. Rev. B **101**, 064303 (2020).

[31] S. M. Rafi-Ul-Islam, Z. B. Siu, C. Sun, and M. B. A. Jalil, Phys. Rev. Appl. **14**, 034007 (2020).

[32] A. Raman and S. Fan, Phys. Rev. Lett. **104**, 087401 (2010).

[33] S. Bittner, B. Dietz, U. Günther, H. L. Harney, M. Miski-Oglu, A. Richter, and F. Schäfer, Phys. Rev. Lett. **108**, 024101 (2012).

[34] T. T. Koutserimpas and R. Fleury, Phys. Rev. Lett. **120**, 087401 (2018).

[35] L. Feng, R. El-Ganainy, and L. Ge, Nat. Photonics **11**, 752 (2017).

[36] S. Malzard, C. Poli, and H. Schomerus, Phys. Rev. Lett. **115**, 200402 (2015).

[37] M. Pan, H. Zhao, P. Miao, S. Longhi, and L. Feng, Nat. Commun. **9**, 1308 (2018).

[38] M. Nakagawa, N. Kawakami, and M. Ueda, Phys. Rev. Lett. **121**, 203001 (2018).

[39] S. Longhi, Phys. Rev. Lett. **105**, 013903 (2010).

[40] S. Rafi-Ul-Islam, Z. B. Siu, C. Sun, and M. bin Abdul Jalil, New J. Phys. **22**, 023025(2020).

[41] S. Rafi-Ul-Islam, Z. Bin Siu, and M. Jalil, Commun. Phys. **3**, 72 (2020).

[42] C. H. Lee, S. Imhof, C. Berger, F. Bayer, J. Brehm, L. W. Molenkamp, T. Kiessling, and R. Thomale, Commun. Phys. **1**, 39 (2018).

[43] N. A. Olekhno, E. I. Kretov, A. A. Stepanenko, D. S. Filonov, V. V. Yaroshenko, B. Cappello, L. Matekovits, and M. A. Gorlach, Nat. Commun. **11**, 1436 (2020).

[44] T. Helbig, T. Hofmann, C. H. Lee, R. Thomale, S. Imhof, L. W. Molenkamp, and T. Kiessling, Phys. Rev. B **99**, 161114(R) (2019).

[45] S. Rafi-Ul-Islam, Z. B. Siu, and M. B. Jalil, Appl. Phys. Lett. **116**, 111904 (2020).

[46] T. Hofmann, T. Helbig, C. H. Lee, M. Greiter, and R. Thomale, Phys. Rev. Lett. **122**, 247702 (2019).

[47] T. Hofmann, T. Helbig, F. Schindler, N. Salgo, M. Brzezińska, M. Greiter, T. Kiessling, D. Wolf, A. Vollhardt, A. Kabaši *et al.*, Phys. Rev. Res. **2**, 023265 (2020).

[48] C. H. Lee and R. Thomale, Phys. Rev. B **99**, 201103(R) (2019).

[49] W. Zhu, Y. Long, H. Chen, and J. Ren, Phys. Rev. B **99**, 115410 (2019).

[50] Y. Eisenberg, Y. Barlas, and E. Prodan, Phys. Rev. Appl. **11**, 044077 (2019).

[51] C. Sun, S M Rafi-Ul-Islam, H. Yang, and M. B. A. Jalil, Phys. Rev. B **102**, 214419 (2020).

[52] C. H. Lee, L. Li, and J. Gong, Phys. Rev. Lett. **123**, 016805 (2019).

[53] W. P. Su, J. R. Schrieffer, and A. J. Heeger, Phys. Rev. Lett. **42**, 1698 (1979).

[54] H. Takayama, Y. R. Lin-Liu, and K. Maki, Phys. Rev. B **21**, 2388 (1980).

[55] J. Sebby-Strabley, M. Anderlini, P. S. Jessen, and J. V. Porto, Phys. Rev. A **73**, 033605 (2006).

[56] E. J. Meier, F. A. An, and B. Gadway, Nat. Commun. **7**, 1 (2016).

[57] E. Pazy and A. Vardi, Phys. Rev. A **72**, 033609 (2005).

[58] M. Fujita, M. Igami, and K. Nakada, J. Phys. Soc. **66**, 1864 (1997).

[59] H.-I. Lu, M. Schemmer, L. M. Aycock, D. Genkina, S. Sugawa, and I. B. Spielman, Phys. Rev. Lett. **116**, 200402 (2016).

[60] H. Schomerus, Opt. Lett. **38**, 1912 (2013).

[61] V. K. Kozin, I. A. Shelykh, A. V. Nalitov, and I. V. Iorsh, Phys. Rev. B **98**, 125115 (2018).

[62] G. Go, I.-S. Hong, S.-W. Lee, S. K. Kim, and K.-J. Lee, Phys. Rev. B **101**, 134423 (2020).

[63] M. Capone, W. Stephan, and M. Grilli, Phys. Rev. B **56**, 4484 (1997).

[64] L. Wang, M. Troyer, and X. Dai, Phys. Rev. Lett. **111**, 026802 (2013).
[65] V. M. Alvarez, J. B. Vargas, and L. F. Torres, Phys. Rev. B **97**, 121401(R) (2018).
[66] K. Yokomizo and S. Murakami, Phys. Rev. Lett. **123**, 066404 (2019).
[67] See Supplemental Material at http://link.aps.org/supplemental/10.1103/PhysRevB.103.035420 for non-reciprocal circuit diagram with unequal directional couplings and admittance dispersion in the complex plane under different boundary conditions.
[68] K. Kawabata, M. Sato, and K. Shiozaki, Phys. Rev. B **102**, 205118 (2020).
[69] S. Yao and Z. Wang, Phys. Rev. Lett. **121**, 086803 (2018).
[70] K. Zhang, Z. Yang, and C. Fang, Phys. Rev. Lett. **125**, 126402 (2020).
[71] N. Okuma, K. Kawabata, K. Shiozaki, and M. Sato, Phys. Rev. Lett. **124**, 086801 (2020).
[72] V. Čerňanová, J. Brenkuš, and V. Stopjakova, J. Electr. Eng. **65**, 283 (2014).
[73] Z. Yang, K. Zhang, C. Fang, and J. Hu, Phys. Rev. Lett. **125**, 226402 (2020).